Single-Molecule Fluorescence Resonant Energy Transfer in Calcium Concentration Dependent Cameleon

Sophie Brasselet,[†,‡] Erwin J. G. Peterman,[†,‡] Atsushi Miyawaki,[§,||] and W. E. Moerner*[,†,‡]

Department of Chemistry and Biochemistry, University of California San Diego, La Jolla, California 92093-0340, Department of Chemistry, Stanford University, Stanford, California 94305-5080, Department of Pharmacology and Howard Hughes Medical Institute, University of California San Diego, La Jolla, California 92093-0647, and Cell Function & Dynamics, Brain Science Institute, RIKEN, 2-1 Hirosawa, Wako, Saitama 351-0198, Japan

Received: November 8, 1999; In Final Form: January 27, 2000

The degree of fluorescence resonant energy transfer in the protein construct "cameleon", whose structure is based on two green fluorescent protein mutants and the calmodulin Ca^{2+}-binding protein, is a sensitive ratiometric reporter of the concentration of Ca^{2+} in solution and cells. For the first time, the detection of single copies of cameleon immobilized in agarose gels is described. This work exemplifies the issues involved in the observation of binding kinetics at the single-molecule level, using fluorescence resonant energy transfer as a signature of the response of the system to the presence of Ca^{2+} ions. The energy transfer distribution deduced from single-molecule fluorescence signals shows an increased width at the Ca^{2+} dissociation constant concentration, which is consistent with the ligand binding kinetics. The complex dynamics of the fluctuations are examined using a combination of autocorrelation and cross-correlation in conjunction with polarization information. We find both negative and positive cross-correlations in the donor and acceptor emission signals, the former related to the energy transfer process, and the latter caused by other perturbations of the donor and acceptor emission.

Introduction

Single-molecule spectroscopy is now recognized as a powerful method of sensing local environments which may be able to provide new insight into biological systems. In particular, the ability to retrieve distributions of heterogeneous properties has provided new information about behavior that is not available from standard ensemble measurements.[1−4] The study of the time trajectories of the emission of naturally fluorescent single proteins[5,6] or single fluorescent probes attached to DNA[7,8] and proteins[9,10] has begun to provide a better understanding of conformational changes and reaction dynamics. Furthermore, the first observation of the excitation transfer between two single molecules in a Förster regime[11] has triggered the use of fluorescence resonance energy transfer[12,13] (FRET) in single donor−acceptor pairs as an interesting tool to study complex systems.[4] This method, sensitive to the distance between two different sites in a given single protein or oligonucleotide, has the potential to reveal new information on structure and dynamics. Single-molecule FRET has been exploited recently at the single-pair level to explore protein dynamics in SNase,[14] DNA cleavage,[15] and RNA folding.[16]

In this paper, we report the observation and analysis of the energy transfer in the cameleon YC2.1 construct, which is based on two mutants of the green fluorescent protein (GFP) and the Ca^{2+}-dependent calmodulin protein.[17,18] As is well-known, the emission of the green fluorescent protein of the jellyfish *Aequora victoria* originates from the spontaneous formation of an emitting chromophore inside a rigid β-barrel structure. Due to its natural fluorescence, GFP has become a powerful tool for cellular biology, and the large number of reported mutations has extended the range of the spectral properties available.[19] The first observations of single copies of GFP, reported for the yellow-emitting phenolate anion mutants,[5,20] described an interesting blinking behavior which has subsequently been extensively studied.[21] The cameleon construct we utilize in this paper, YC2.1, is formed from the sequential fusion of five poly(peptides): (a) an enhanced cyan GFP mutant "ECFP" (F64L/S65T/Y66W/N146I/M153T/V163A/N164H), (b) calmodulin, (c) a glycylglycine linker, (d) M13, a peptide composed of the calmodulin-binding domain of myosin light chain kinase, and (e) an enhanced yellow mutant of GFP, EYFP-V68L/Q69K (S65G/V68L/Q69K/S72A/T203Y). The binding of calcium ions to the four binding sites of calmodulin stimulates a strong binding interaction with the M13 peptide and a change of conformation of the whole system toward a more compact structure.[22] The resulting energy transfer from the cyan donor GFP to the yellow acceptor GFP is therefore improved by the decrease of their relative distance and possibly also by changes in orientation. Of particular interest here is the advantage afforded by ratiometric detection of the donor and acceptor emission signals, which renders the measurement insensitive to absolute emission values. Energy transfer in YC2.1 has been used to observe calcium transients in HeLa cells,[17,18] and to record ratiometric images of $[Ca^{2+}]$ changes in cardiac myocytes using two-photon excitation.[23]

A detailed study of the dynamics and efficiency of the energy transfer between the two GFP mutants in single YC2.1 cam-

* To whom correspondence should be addressed: W. E. Moerner, Department of Chemistry, Stanford University, Stanford, CA 94305-5080. Email: w.e.moerner@stanford.edu. Tel: (650) 723-1727; Fax: (650) 725-0259.

† University of California at San Diego.

‡ Stanford University.

§ Howard Hughes Medical Institute.

|| Brain Science Institute.

10.1021/jp993954o CCC: $19.00
Published on Web 03/23/2000

eleons is described in this paper. We use confocal microscopy to measure the emission in two spectral bands for single copies of the construct immobilized in water-filled agarose gels. We observe fluctuations in the energy transfer, which are attributed to the binding kinetics of the ligand and other local perturbations. The distribution of the energy transfer efficiency shows furthermore a clear dependence on the calcium concentration in the medium, which is a signature of the degree of conformational changes in the structure upon calcium binding. Different issues relating to the observation of FRET in single molecules are addressed. First, the emission properties of the GFP mutants involved in the YC2.1 cameleon are shown to be a critical limitation in the observation of fluorescence of single cameleons. Second, the time averaging of the different dynamic processes occurring in the system has to be taken into account in order to understand the observed distributions and fluctuations.

Experimental Section

Proteins and Sample Preparation. For single-molecule measurements, the proteins were diluted to very low concentration (typically 10^{-10} M) in agarose gels, to limit translational diffusion without restraining rotation in the relatively large aqueous pores ($\sim$200 nm[24]). Agarose gels were made from a heated (70 °C) solution of 1% (w/v) low-melting point agarose (Boehringer Mannheim) and 0.1% (w/v) sodium azide in pH 7.5 (100 mM HEPES (4-(2-hydroxyethyl)-1-piperazineethanesulfonic acid), 50 mM KCl) buffer. A small amount of the protein diluted in buffer was added to this liquid solution after it had cooled to 40 °C. A 2 μl aliquot of the final protein solution was pipetted between two cover slips and allowed to cool to room temperature to form the gel.

The GFP mutants EYFP (S65G/S72A/T203Y), ECFP, and the YC2.1 cameleon complex were produced by standard recombinant techniques described previously.[17] The expression, bulk spectroscopic characterization, and calcium titration curves of the YC2.1 complex have been detailed in previous studies.[17,18] In particular, Ca^{2+} titration curves of YC2.1 evidenced a biphasic [Ca^{2+}] change of the ratio between the acceptor and donor emission intensities, with apparent dissociation constants K_d of 100 nM and 4.3 μM, and respective Hill coefficients of 1.8 and 0.6. To obtain the required calcium concentration in the final gel, YC2.1 stored in 0.2 mM [Ca^{2+}] pH 7.5 (100 mM HEPES, 50 mM KCl) buffer was diluted with the proper EDTA (ethylenediamine tetraacetic acid) concentration. Absolute determinations of [Ca^{2+}] require in general careful accounting of various factors, such as the pH dependence of the binding equilibrium, the possibility of Ca^{2+} contamination from buffer solutions, and any perturbations from the agarose gel host. In this paper, the focus is on the primary effect of large concentration changes rather than precise absolute concentrations, therefore, we chose three main regimes for study: low [Ca^{2+}], intermediate [Ca^{2+}], and high [Ca^{2+}]. Titrations to achieve low ([Ca^{2+}] $\ll$ 0.01 μM, achieved with 200 μM EDTA) and high concentration ([Ca^{2+}] $\approx$ 0.2 mM) are not difficult. To experimentally calibrate our intermediate concentration, we utilized the published titration of the acceptor/donor emission ratio change versus [Ca^{2+}] mentioned above. Specifically, we prepared a sample with an approximate concentration near the dominant first K_d value of 0.1 μM, then used this to make a high-cameleon-concentration sample in agarose, and measured the (bulk) acceptor/donor emission ratio in our confocal microscope. Comparison of this ratio to the corresponding ratio for bulk Ca^{2+}-saturated and Ca^{2+}-free samples yielded a normalized change in the ratio of 46 $\pm$ 16% (three trials). From the published titration curve,[18] the actual concentration range corresponding to our measured ratio change is 0.1$-$1 μM. This sample will be denoted intermediate Ca^{2+} concentration for the remainder of this paper.

Confocal Microscope Setup. The optical beam of a 442 nm HeCd laser (Liconix) was directed to the sample plane via the epi-illumination path of an inverted microscope (Nikon Diaphot 200) by a dichroic mirror (455DCLP Omega Optical), and then focused on the sample using a Nikon 60 $\times$ 1.4 NA PlanApo oil immersion objective. The incoming beam was circularly polarized at the sample plane, with a typical intensity of 400 W/cm^2. The fluorescence signal passing through the dichroic was focused on a pinhole of 50 μm diameter for confocal imaging. The pinhole was then imaged with 50.8 mm focal length lenses on two avalanche photodiodes (SPCM 50 and 25 cps dark counts, EG&G) by splitting the beam using a long pass dichroic (515DRLP, Omega Optical) or a polarizing beam splitter cube, depending on the type of measurement performed. The residual excitation light was suppressed by an adequate set of band-pass filters (535DF25 for the yellow mutant and 480DF50 for the cyan mutant, Omega Optical). A computer-controlled piezoelectric scanner (Thermomicroscopes Lumina) performed the two-dimensional scanning of the sample stage, over a typical area of 10 μm $\times$ 10 μm with a 100 $\times$ 100 pixels resolution. A digital counting board (PC-TIO10, National Instruments) in a second computer simultaneously recorded the photon counts of the two APDs, with a typical integration time of 20 ms.

Results and Discussion

Observation of Single Copies of YC2.1. In a typical experiment, a first scan of a 10 μm $\times$ 10μm area of the sample containing the molecules diluted in agarose gel was performed with a speed of 10 μm/s, to locate the bright, isolated, diffraction-limited ($\sim$300 nm diameter) spots characteristic of the presence of single fluorescent species. The sample stage was then translated to each spot individually and the time dependence of the emission from a single molecule was recorded using two-color photon counting at a 50 Hz rate. Preliminary calibration information was obtained by measuring the individual dynamic behavior of the ECFP cyan and EYFP yellow mutants during excitation at 442 nm. A typical time trace of the ECFP donor mutant shown in Figure 1a exemplifies the single emitter signature by the abrupt drop of the signal, characteristic of the bleaching of the chromophore. The thick line in Figure 1 represents the emission centered at 480 nm (donor channel) and the thin line the emission signal centered at 535 nm (acceptor channel). The emission of the single molecule begins when ECFP apparently recovers from a previous (reversible) photobleaching or blinking event as described in ref 21. The recording of many time traces of this type revealed a nonnegligible amount of leakage of the donor emission into the acceptor channel, which was predictable from the large width of the emission spectrum of ECFP in solution. This leakage fraction is critical to quantify the effective emission signal of the acceptor in the study of the cameleon construct below. Another important characteristic of the measured time traces was the relatively short on-time of the emission events before photo-bleaching, which will be discussed in the next section.

Using the same conditions of excitation, we performed single-molecule measurements on the isolated yellow EYFP mutant, which is slightly different from the acceptor variant of GFP used in the cameleon construct, but has similar fluorescence

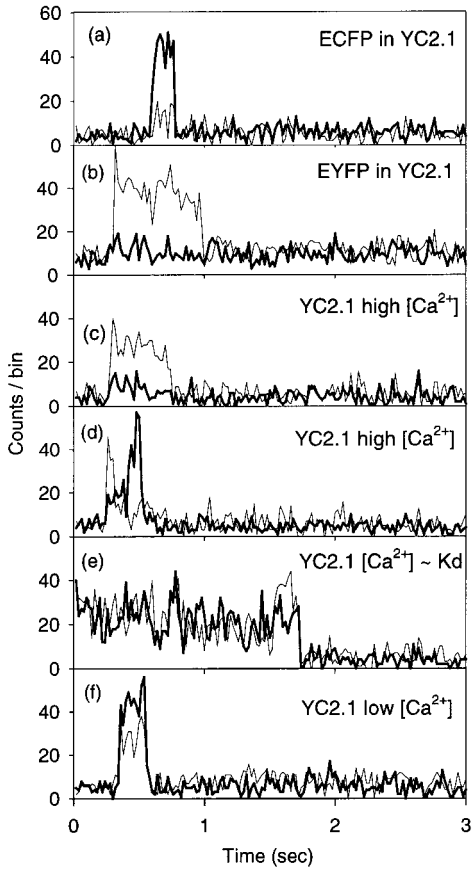

Figure 1. Typical two-wavelength time trajectories of different single molecules diluted in agarose gel. The thick continuous line is the donor emission intensity measured at 480 nm, the thin line the acceptor intensity measured at 535 nm. (1a) isolated ECFP, (1b) isolated EYFP, (1c, 1d) YC2.1 at high calcium concentration, (1e) YC2.1 at intermediate calcium concentration, (1f) YC2.1 at low calcium concentration. The excitation wavelength is 442 nm, and the incident intensity 400 W/cm^2, except for Figure 1b where it has been increased to 1.6 kW/cm^2. The integration time is 20 ms.

properties. No visible signal was observed with 442 nm-excitation wavelength in either the donor or the acceptor emission channels, showing that significant direct excitation of the acceptor by the incident beam was unlikely in the cameleon complex under these conditions. However a noticeable level of emission signal was detectable in the acceptor channel using four times higher excitation intensity, as shown in Figure 1b.

We measured time traces of single copies of YC2.1 cameleon at a relatively low excitation intensity of typically 400 W/cm^2, for the three different concentrations of calcium in agarose gel that we investigated, namely Ca^{2+} saturation, intermediate Ca^{2+} concentration, and Ca^{2+}-free samples. Figure 1c and d were measured in the case of high calcium concentration. The short on-time event observed for both channels in Figure 1c is representative of the majority of the recorded time traces for the three different calcium concentrations. The acceptor level of signal in Figure 1c is significantly higher than the donor signal, showing a high amount of excitation transfer from the cyan to the yellow mutant. Both signals drop simultaneously at ~1 s, which we believe is due to the bleaching of the donor first which immediately cancels the acceptor emission. A similar level of excitation transfer can be initially observed in Figure 1d, except that for this molecule the acceptor bleaches first at 0.4 s, leading to a significant increase of the donor signal due to the recovery of the energy previously transferred to the acceptor, followed by bleaching of the donor. Figure 1e is measured at the intermediate calcium concentration, and is coincidentally one of the longest time traces measured. This time trace shows significant fluctuations in the emission of both channels. These fluctuations arise from complex dynamics that will be discussed below. Most other time traces recorded at this intermediate calcium concentration showed shorter on-times similar to Figure 1c. Short on-times were also dominant at low calcium concentration, as exemplified in Figure 1f. In this case, the level of the emission signal of the donor is clearly higher than the emission of the acceptor, as expected from a low energy transfer.

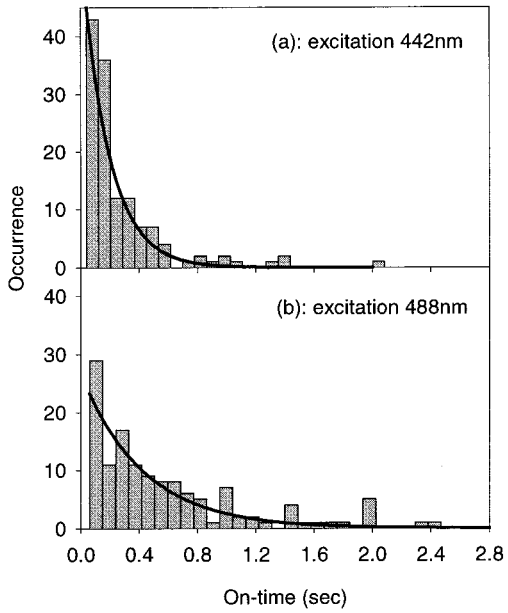

Figure 2. Histograms of the on-times of time trajectories for single copies of YC2.1 at two excitation wavelengths, 442 nm (2a) and 488 nm (2b). The on-time in the case of the 442 nm excitation was defined as the simultaneous on-time of the 480 nm and 535 nm detection channels before any bleaching event. The detected signal in the 488 nm excitation case was the 535 nm channel. The excitation intensity was 400 W/cm^2 for both excitation wavelengths. The time constant of the exponential decays (solid curves) are (185 ± 16) ms and (480 ± 30) ms for the a and b panels, respectively.

The recorded time traces showed on-time durations ranging from 60 ms to 2 s, followed by the drop of one or both signals. Unfortunately, since the off-times are apparently very long (≳ 100 s, see ref 21), the data from only one on-time per molecule could be analyzed. On-times were measured for ~150 single copies of cameleon and reported in the histogram shown in Figure 2a in the case of the intermediate calcium concentration. This histogram was fit by a single exponential with a time decay of (185 ± 16) ms, which is relatively short and representative of the average of the observed on-times in GFP single molecule experiments.[21] However, the same system excited at 488 nm from an argon-ion laser with the same incident intensity results in a much longer exponential decay time of (480 ± 30) ms (Figure 2b). In this case, only the EYFP acceptor component of YC2.1 was excited, which allowed exploration of the time behavior of the fused yellow mutant independently. The yellow mutant excited independently clearly possesses a lower bleaching rate than the ECFP mutant. This confirms that the bleaching events and the very high number of trajectories with short on-times observed in Figure 1c, 1d, and 1f for YC2.1 are mostly governed by the early bleaching of the ECFP mutant.

Histogram of the Estimated Excitation Transfer Efficiencies for Different Ca^{2+} Concentrations. Due to the short on-time of the majority of the time traces arising from the donor

photophysics, only a few time trajectories showed a first bleaching of the acceptor followed by the subsequent increase in the emission of the donor mutant (as in Figure 1d). This situation allows in principle direct evaluation of the FRET efficiency from the recovery of the emission by the donor, but was uncommon for the YC2.1 construct. In practice, we measured the I_A/I_D ratio between the time averages of the means of the two signals before any bleaching event, I_D being the intensity of the donor measured at 480 nm and I_A the intensity of the acceptor measured at 535 nm. The distribution and dynamics of this ratio for individual molecules contain additional information on the energy transfer process that may not be available from an ensemble measurement. An estimated FRET efficiency was deduced from this ratio, whereby both intensities were corrected for the wavelength dependence of the detection efficiency and the quantum yields of each mutant. The final estimated FRET efficiency, E, was calculated from the corrected intensities I_A^{corr} and I_D^{corr}:

$$E = \frac{I_A^{corr}}{I_A^{corr} + I_D^{corr}} = \frac{1}{1 + \frac{\phi_A}{\phi_D}\frac{D}{\left(\frac{I_A}{I_D} - L\right)}} \quad (1)$$

where D is the ratio between the different detection efficiencies at the 535 nm and 480 nm wavelengths, which was estimated to be 1.43 accounting for the filters and dichroics used in the confocal experiment. L is the proportion of the donor signal I_D leaking into the acceptor channel (0.25), as determined from time traces on single copies of ECFP diluted in agarose gel. This value matches that obtained by a direct measurement of the ECFP emission spectrum in a bulk solution in the microscope. ϕ_D and ϕ_A are the quantum yields of the donor and acceptor, 0.4 and 0.7, respectively, as determined from bulk experiments.[19]

This definition of the *estimated* FRET efficiency (eq 1) assumes that the fluorescence quantum yields of the GFP mutants in the YC2.1 complex are the same as the mutants separately. In practice, these values could be slightly different due to the effect of the fusion of the proteins to calmodulin and the M13 peptide domain, and a modification to the correction factor D would be necessary to evaluate the *absolute* energy transfer efficiency of the system.

The transfer efficiency defined in eq 1 was evaluated for a large number of single YC2.1 molecules for the three different calcium concentrations and plotted in the histograms shown in Figure 3. The means of the distributions, representing the average transfer efficiencies, clearly depend on [Ca^{2+}] and have values of 0.6, 0.47, and 0.4 at high, intermediate, and low calcium concentrations. These values are in relatively good agreement with the I_A/I_D ratio measured in experimental ensemble data.[18] However, our single-copy measurement provides further insight into the nature of the system, since we obtain full distributions. In particular, the histograms show relatively large widths with the largest width at the intermediate calcium concentration, the standard deviations of the distributions being 0.09, 0.17, and 0.12 from high to low calcium concentration. The observed width at intermediate calcium concentration clearly exceeds the contribution of instrumental noise, as shown in the solid lines of Figure 3. The noise calculation includes the shot noise effect, calculated from the inverse square root of the relative variations in the signal[15] with a finite number of detected photons of ~60 counts/bin, and the experimental background noise originating from scattering and fluorescence of the gel and substrate.

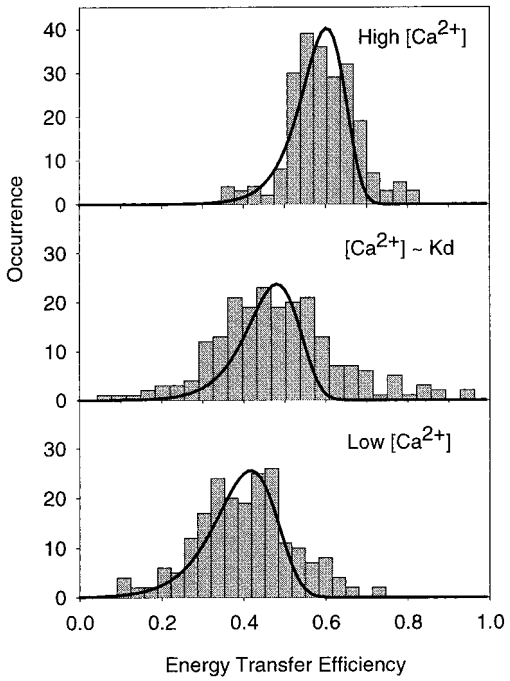

Figure 3. Histograms of the estimated energy transfer efficiency as defined in eq 1, deduced from single-copy measurements of YC2.1 for three different concentrations of calcium: (a) at Ca^{2+} saturation, (b) at intermediate concentration, and (c) for a calcium-free agarose gel. The solid lines are the expected energy transfer efficiency distribution from the experimental noise, including shot noise and background noise as explained in the text.

To understand the excess width of the distribution at intermediate [Ca^{2+}], one must consider the different parameters that could affect the transfer efficiency in the YC2.1 construct. First of all, since the amount of energy transfer is dependent on [Ca^{2+}], one obvious source for fluctuations is the kinetics of Ca^{2+} binding. Separate ensemble stopped-flow measurements on YC2.1 yield an upper bound for the off-rate k_{off}, of (2.4 ± 0.3) sec^{-1} (Geoff Baird and R. Y. Tsien, unpublished private communication). Therefore, at the K_d concentration representative of half-saturation, the observed rate would be (200 ± 25 $ms)^{-1}$. The corresponding rate for our intermediate calcium concentration, which is around $2 \times K_d$, should be slightly higher than this last value. Since this process has a timescale close to our overall observation time dictated by the *emission* on-time of each cameleon molecule, one would expect larger variations in the measured E values from molecule to molecule. In other words, the kinetic parameters suggest that the degree of energy transfer fluctuates more, thus the observed E values show more variation from molecule to molecule. At high [Ca^{2+}], the binding rate is so fast that the unbound state is seldom observed during our observation time, so that the variations of E are smaller, while at low [Ca^{2+}], the unbound state is predominantly observed during the emission on-time. In fact, the single-molecule event shown in Figure 1d might even be due to Ca^{2+} ion unbinding, but this can only be a suggestion without improved statistics.

To obtain further understanding of the influence of the binding/unbinding dynamics on the observed effect, we now consider some of the relevant parameters that can influence the excitation transfer process: the orientation[13] of the two dipoles of the GFP chromophores, and their relative distance within the cameleon structure.

Orientation Effects. Two different classes of experiments have been performed in order to investigate the orientation of both GFPs fused to the cameleon construct. We first report single-molecule polarization measurements, to ensure that the system is free to rotate in the agarose pores. This type of measurement furthermore provides the orientation information for each chromophore independently in agarose gels, averaged on the 20 ms timescale of our measurement. Second, steady-state anisotropy studies in bulk solutions are described in order to obtain faster timescale information on the orientational diffusion times of the GFPs fused to cameleon. We finally discuss these results in the context of the energy transfer measurements.

We first studied the polarization behavior of the fluorescence of single copies of YC2.1 cameleons in order to estimate the orientational flexibility of the cyan and yellow mutants. In the confocal geometry, the choice of a circularly polarized excitation beam allows photoexcitation of almost all molecules independent of their orientation or orientational dynamics, and the orientation information is retrieved by analyzing the fluorescence signal along two orthogonal polarization axes simultaneously.[8] The polarization is defined as $P = (I_x - I_y)/(I_x + I_y)$, with I_X and I_Y the emission intensities of the two polarization components of the projection dipole along the X and Y axes of the sample plane. Assuming that the incident polarization is perfectly circular and that the excitation and emission dipoles are parallel, the resulting distribution of the polarization measured for many single molecules is a histogram centered at a mean value $\langle P \rangle = 0$. For a set of molecules undergoing a fast rotation at all orientation angles during the measurement timescale, P is averaged and therefore takes a unique value $P = 0$. In practice, the width of the distribution of P has a lower limit defined by the noise-induced fluctuations in the signal of the two polarization channels. More importantly, if the chromophores tumble slowly during the measurement integration time, the resulting histogram will broaden with peaks at $P = \pm 1$ for the extreme case of fixed orientations.

Similar information can be retrieved by a modulation of the excitation polarization between the two X and Y directions, the detection being unpolarized.[8] This situation is in principle convenient to retrieve simultaneous angular information at two different emission wavelengths in FRET, and therefore allows the direct measurement of the relative angle between the two dipoles. However in practice, only very stable chromophores have a sufficiently long on-time to cover several periods of the polarization modulation. In the case of the YC2.1 cameleon, the short on-time of the time traces forced us to choose the circular polarization configuration.

Two separate single-molecule polarization measurements were performed at the two detection wavelengths 480 nm and 535 nm, allowing retrieval of orientation information of both acceptor and donor. The histograms of the polarization for single cameleons at both wavelengths, shown in Figure 4a and 4b, are centered on 0, as expected from the circularly polarized excitation. The widths of these histograms are very close to the width obtained from the same measurement of the isolated ECFP mutant diluted in agarose, shown in Figure 4c. The width of the histograms in Figure 4 is found to be very close to the limit introduced by the noise in the measurement, whose root-mean-square estimation is $\Delta P = 0.19$. This noise calculation includes the shot noise effect and the experimental background noise. This result shows a high degree of rotational freedom of the system at the 20 ms timescale. However at this stage, this fast rotation can either be governed by a GFP rotation in the cameleon complex or by a fast rotation of the whole cameleon in the pore with GFPs fixed in the construct, or a combination of both effects.

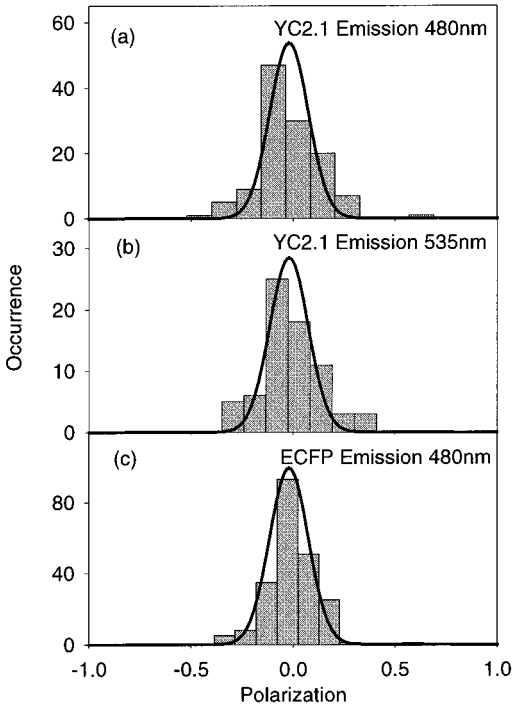

Figure 4. Histograms of the polarization P as defined in the text, measured separately from single-copy measurements of YC2.1 at the donor and acceptor emission wavelengths, respectively 480 nm (a) and 535 nm (b), both with pumping at 442 nm. (c) represents the histogram resulting from similar polarization measurements on ECFP alone, with an emission wavelength of 480 nm. The solid lines in each figure are the expected noise limited distribution from an ensemble of freely and fast rotating molecules. The noise effect includes the shot noise and the experimental background noise.

To explore this last point, we performed steady-state anisotropy measurements in solution. Conventional bulk steady-state polarization anisotropy measurements in a fluorimeter give critical additional information related to the rotational diffusion time as compared to the fluorescence lifetime of the chromophores. In previous studies of the GFP mutant S65T in buffer solution, the following properties were measured:[25] emission lifetime 2.93 ± 0.02 ns, rotational correlation time 20 ± 1 ns, and initial anisotropy $r_o \approx 0.37$. The rotational correlation time of the Ca^{2+}-loaded YC2.1, estimated from the crystal structure of the calmodulin-M13 complex[26] and GFP,[27] is expected to be 100 times larger than the GFP fluorescence lifetime. Therefore if GFP is immobilized in the cameleon construct, one would expect a steady-state anisotropy close to 0.37. Using a solution of Ca^{2+}-loaded YC2.1 excited at 442 nm, we measure the steady-state anisotropy of the fused ECFP emission to be 0.3 ± 0.01, which is close to the anisotropy value of the free ECFP in solution (0.29 ± 0.015). Similarly, when excited at 488 nm, EYFP fused to cameleon has an anisotropy of 0.3 in both Ca^{2+}-loaded and Ca^{2+}-free cases. The emission from EYFP pumped via the ECFP has a much lower anisotropy of 0.15, which is characteristic of the transfer from the donor. These steady-state anisotropy values for ECFP and EYFP show that both mutants have a nonnegligible degree of rotational freedom in the cameleon construct at ms timescales.

Returning to the single-molecule regime, time-dependent studies of the polarization ratio P for both GFPs in cameleon gave additional information on their *apparent* orientation dynamics at the 20 ms timescale of our measurement. We

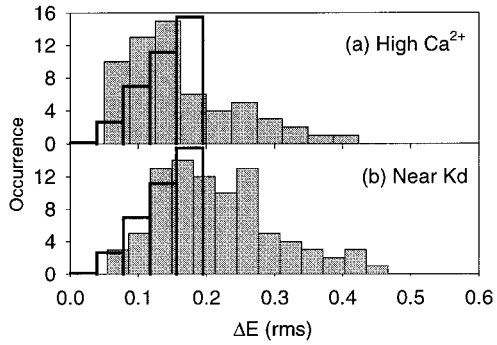

Figure 5. Histograms of ΔE, the rms amplitude of the fluctuations of the energy transfer efficiency E as defined in eq 1, as determined from the recorded time trajectories in the case of high (a) and intermediate (b) calcium concentration (shaded). The additional superposed solid line histogram represents the upper limit of the energy transfer fluctuations that might be expected from noise effects alone as follows: as E is deduced from the intensities I_A and I_D, ΔE contains both shot noise (with an average level of the total signal $I_A + I_D$ of 50 counts/bin) and background noise effects (with a background mean level of 5 counts/bin). To estimate the theoretical ΔE upper limit value, we approximately accounted for the effects of varying time trajectory length $T = N\lambda$ (T is the on-time for a single molecule, $\tau = 20$ ms is the integration (bin) time, N is the number of bin times within T). As usual, for random noise, the ΔE distribution should scale as $\sqrt{N}$. The resulting histogram is computed by combining the histograms that we would obtain from the average on-time ($N = 10$) and from the shortest on-time ($N = 1$). Although this analysis does not include detailed statistics from the on-time distribution, it gives a reasonable estimation of the upper limit of the expected ΔE values.

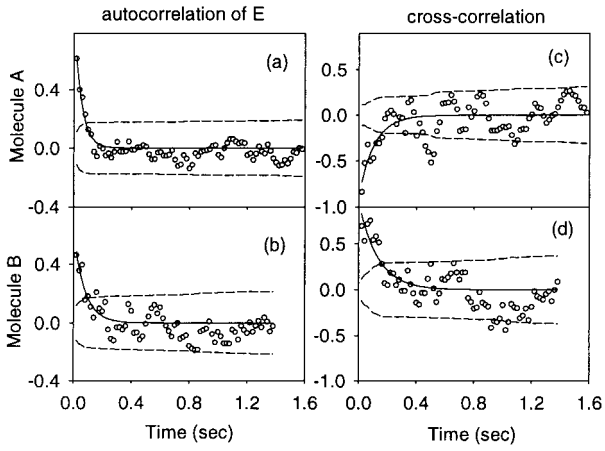

Figure 6. (a, b): Autocorrelation of E values defined in eq 1 measured for a long time trajectory in the case of intermediate calcium concentration for two molecules A (a) and B (b). The characteristic times of the exponential decays are (48 ± 7) ms (a) and (80 ± 13) ms (b). (c, d): cross-correlation of the I_A and I_D signals for molecules A (c) and B (d). The time constants of the exponential fits are (106 ± 27) ms (c) and (130 ± 30) ms (d). The confidence limits on the autocorrelations are shown as dashed lines on both traces.

calculated the temporal autocorrelation of polarization ratios measured for several long on-time trajectories ($\sim$1−2 s) in YC2.1 similar to Figure 1d. The polarized time trajectories show a very fast decay of correlation (<10 ms) for both GFPs, which confirms the fact that independent orientation fluctuations in the system are most likely to be averaged over the 20 ms integration time. The effect of the orientation fluctuations on the time fluctuations of the energy transfer is presented in the next section.

Fluctuations of the Energy Transfer. The root-mean-square (rms) values of the temporal fluctuations in the energy transfer E, ΔE, deduced from the recorded time trajectories, are represented in histograms in Figure 5 for high and intermediate calcium concentration. This figure exemplifies large rms fluctuations, especially in the case of the intermediate concentration (note the shift to higher values in Figure 5b). We compared the observed effect to the fluctuation amplitude expected from the noise in the measurement. The noise fluctuation limit, represented in the superposed histograms in Figure 5 as dark lines, has been computed from the shot noise effect,[15] corrected for the experimental background noise. It appears that the fluctuations observed for both concentrations exceed the noise limit, with more ΔE values with larger ΔE in the intermediate concentration case. The background noise contains in particular any fluctuations originating from the laser. We investigated the timescale of laser fluctuations by calculating the autocorrelation of background signals after some bleaching event. The time decay characteristic of this autocorrelation was much faster than the integration time of the measurement, showing that the laser fluctuations are not a major source of measurable variations in the emission intensity in the acceptor and donor channels.

To explore the origin of these fluctuations further, we calculated correlations of the longest time trajectories, namely with on-time durations of 1 to 2 s. Two correlations are relevant: the autocorrelation of the E factor deduced from the I_A/I_D ratio, as well as the cross-correlation between the I_A and I_D time trajectories. In contrast with autocorrelation analysis, cross-correlation allows discrimination between positive and negative correlations of the donor and acceptor signals, which contains important information on the nature of the fluctuations. Two examples of such correlations are depicted in Figure 6 in the case of single YC2.1 cameleons at intermediate calcium concentration.

The autocorrelation decays in the energy transfer value have been measured over 8 long time trajectories and show an averaged decay time of (60 ± 20) ms. These apparent slow variations might have different origins, among which the dynamics of the Ca^{2+} binding/unbinding equilibrium plays an important role. However, other parameters might screen the binding kinetics effect in the observed fluctuations, in particular the orientational dynamics of the dipoles in the cameleon construct.

We demonstrated in the previous section that the timescale of orientation fluctuations of the GFPs taken independently was very fast compared to the measurement integration time, but slow compared to the fluorescence lifetime. We assume that the relative angle between the dipoles follows the same dynamics (which would be the case if the orientations of the GFP dipoles are not correlated in the system). Since the actual excitation rate in our system is on the order of 10^5/s, it is reasonable to assume that the two fluorophores should be able to find a new relative orientation between each FRET event, resulting in fast fluctuations of E. However, these fluctuations are averaged away during the 20 ms integration time and would not participate to the slower variations observed for E in Figure 1d for example.

Although in this study the number of long time trajectories is low, it is interesting to note that among these traces both positive and negative correlations could be observed (Figure 6c and 6d). In a pure energy transfer process, the cross-correlation would be negative with the same time constant as the autocorrelation of E. It appears that the energy transfer seems to take place along with another competing process, responsible for some degree of positive correlation. This explains in particular the discrepancy between the decay times of the autocorrelation of E (48 ± 7) ms (Figure 6a) and (80 ± 13) ms (Figure 6b), and the time constant of the cross-correlations

(Figure 6c and 6d), which are respectively (106 ± 27) ms and (130 ± 30) ms. The exact origin for the observed positive cross-correlation is not identified at this stage, but might be assigned to an external perturbation of the energy transfer equilibrium, which introduces some fluctuations in the overall number of photons emitted by the (donor + acceptor) system. We performed a simple simulation, which shows that experimental artifacts such as the leakage from the donor channel into the acceptor channel or possible drifts in the laser intensity are unlikely to generate dominant positive correlation. Different other sources of positive correlations are possible. For instance, any independent variation in the emission quantum yield of the donor and/or acceptor is likely to induce such correlations. In the case of GFP, the quantum yield has been shown to be very sensitive to the surrounding environment[28] and may involve conformational rearrangement of the GFP-chromophore, as observed in fluorescence correlation studies[29] and quantum chemical calculations.[30,31] Changes in the emission and absorption spectral overlap may also be involved.

It is interesting to note that the fluctuation time constants are calcium concentration dependent. At high calcium concentration, we observed much shorter time constants both for the autocorrelation of *E*, as well as for the cross-correlation signals (5−25 ms). This observation is consistent with the decrease in the width of the ΔE histogram at high calcium concentration (Figure 5a), whereby the fluctuations might be further averaged. Although the small number of long on-time trajectories do not allow statistics on the cross-correlation time constant, these results suggest that the observed fluctuations depend on the conformation of the intervening calmodulin−M13 framework. In particular, the few positive cross-correlation time constants that we measured are of the same order of magnitude as the rate constants obtained from bulk stopped-flow measurements. In summary, the anticorrelated fluctuations of Figure 6 along with the energy transfer histogram of Figure 3 and the varying widths of the ΔE distributions in Figure 5, are partly a signature of the dynamics of the response of single YC2.1 cameleons to the presence of calcium and the binding and unbinding kinetics. The observation of positive cross-correlations from an unknown source indicates that fluctuations of *E* should be interpreted with care; in particular, it is not possible to ascribe the fluctuations only to variations in the distance between the two fluorophores.

Conclusion

Analysis of single-molecule signals from the cameleon YC2.1 complex diluted in aqueous gels allows retrieval of several features of the energy transfer between the donor and acceptor mutants of the construct, depending on the calcium concentration in the medium. Beside the reorientation fluctuations of the two dipoles that seem to occur on a fast timescale compared to the measurement timescale, we detected slower variations in the energy transfer between the two GFP mutants. Cross-correlation analyses allowed us to uncover a nonnegligible degree of positive correlation between the donor and acceptor emission signals for some single molecules. The anti-correlated component of the fluctuations is mainly assigned to variation in the energy transfer between the donor and acceptor, as a result of the slow dynamics of the response of the system to the presence of calcium. The large width in the histogram of energy transfer at the intermediate calcium concentration may furthermore originate from a coincidence of the measurement time with the binding kinetics of calcium ions. This work demonstrates that single cameleons do not directly act as accurate calcium concentration reporters, because the degree of energy transfer from copy to copy shows a large range of values among the different members of the population. Nevertheless, study of individual cameleon copies has yielded new data on fluctuations in energy transfer which do depend on the local calcium concentration, and the enumeration of all sources of the fluctuations must be the subject of future study. Clearly longer on-times would be preferable to understand the different correlated and anti-correlated processes present in this system. In any case, these studies illustrate that single-molecule FRET experiments on cameleon may be useful in exploring the dynamics of the formation of tertiary structures in the folding of proteins.

Acknowledgment. We thank R.Y. Tsien, S. Kummer, and S. Woutersen for helpful discussions. This work was supported in part by National Science Foundation Grant Nos. DMR-9612252 and MCB-9816947.

References and Notes

(1) Nie, S. M.; Zare, R. N. *Ann. Rev. Biophys. Biomol. Struct.* **1997**, *26*, 567−596.
(2) Xie, X. S.; Trautman, J. K. *Ann. Rev. Phys. Chem.* **1998**, *49*, 441−480.
(3) Moerner, W. E.; Orrit, M. *Science* **1999**, *283*, 1670−1676.
(4) Weiss, S. *Science* **1999**, *283*, 1676−1683.
(5) Dickson, R. M.; Cubitt, A. B.; Tsien, R. Y.; Moerner, W. E. *Nature* **1997**, *388*, 355.
(6) Lu, H. P.; Xun, L. Y.; Xie, X. S. *Science* **1998**, *282*, 1877−1882.
(7) Ha, T.; Enderle, T.; Chemla, D. S.; Selvin, P. R.; Weiss, S. *Phys. Rev. Lett.* **1996**, *77*, 3979−3972.
(8) Ha, T.; Glass, J.; Enderle, T.; Chemla, D. S.; Weiss, S. *Phys. Rev. Lett.* **1998**, *80*, 2093−2096.
(9) Vale, R. D.; Funatsu, T.; Pierce, D. W.; Romberg, L.; Harada, Y.; Yanagida, T. *Nature* **1996**, *380*, 451.
(10) Sase, I.; Miyata, H.; Ishiwata, S.; Kinosita, K. *Proc. Natl. Acad. Sci. U.S.A.* **1997**, *94*, 5646−5650.
(11) Ha, T.; Enderle, T.; Ogletree, D. F.; Chemla, D. S.; Selvin, P. R.; Weiss, S. *Proc. Natl. Acad. Sci. U.S.A.* **1996**, *93*, 6264−6268.
(12) Stryer, L.; Haugland, R. P. *Proc. Natl. Acad. Sci. U.S.A.* **1967**, *58*, 719−726.
(13) Clegg, R. M. Fluorescence Resonance Energy Transfer. In *Fluorescence Imaging and Microscopy*; X. F. Wang, B. H., Ed.; Wiley-Interscience: New York, 1996; Vol. 137, p 179.
(14) Ha, T. J.; Ting, A. Y.; Liang, J.; Caldwell, W. B.; Deniz, A. A.; Chemla, D. S.; Schultz, P. G.; Weiss, S. *Proc. Natl. Acad. Sci. U.S.A.* **1999**, *96*, 893−898.
(15) Deniz, A. A.; Dahan, M.; Grunwell, J. R.; Ha, T. J.; Faulhaber, A. E.; Chemla, D. S.; Weiss, S.; Schultz, P. G. *Proc. Natl. Acad. Sci. U.S.A.* **1999**, *96*, 3670−3675.
(16) Ha, T. J.; Zhuang, X.; Kim, H. D.; Orr, J. O.; Willamson, J. R.; Chu, S. *Proc. Natl. Acad. Sci. U.S.A.* **1999**, *96*, 9077.
(17) Miyawaki, A.; Llopis, J.; Heim, R.; McCaffery, J. M.; Adams, J. A.; Ikura, M.; Tsien, R. Y. *Nature* **1997**, *388*, 882−887.
(18) Miyawaki, A.; Griesbeck, O.; Heim, R.; Tsien, R. Y. *Proc. Natl. Acad. Sci. U.S.A.* **1999**, *96*, 2135−2140.
(19) Tsien, R. Y. *Ann. Rev. Biochem.* **1998**, *67*, 509−544.
(20) Pierce, D. W.; HomBooher, N.; Vale, R. D. *Nature* **1997**, *388*, 338−338.
(21) Peterman, E. J. G.; Brasselet, S.; Moerner, W. E. *J. Phys. Chem. A* **1999**, *103*, 10 553−10 560.
(22) Martin, S. R.; Bayley, P. M.; Brown, S. E.; Porumb, T.; Zhang, M. J.; Ikura, M. *Biochemistry* **1996**, *35*, 3508−3517.
(23) Fan, G. Y.; Fujisaki, H.; Miyawaki, A.; Tsay, R. K.; Tsien, R. Y.; Ellisman, M. H. *Biophys. J.* **1999**, *76*, 2412.
(24) Rees, D. A. *Biochem. J.* **1972**, *126*, 257−273.
(25) Swaminathan, R.; Hoang, C. P.; Verkman, A. S. *Biophys. J.* **1997**, *72*, 1900−1907.
(26) Krueger, J. K.; Bishop, N. A.; Blumenthal, D. K.; Zhi, G.; Beckingham, K.; Stull, J. T.; Trewhella, J. *Biochemistry* **1998**, *37*, 17 810−17 817.
(27) Ormo, M.; Cubitt, A. B.; Kallio, K.; Gross, L. A.; Tsien, R. Y.; Remington, S. J. *Science* **1996**, *273*, 1392−1395.
(28) Kneen, M.; Farinas, J.; Li, Y. X.; Verkman, A. S. *Biophys. J.* **1998**, *74*, 1591−1599.
(29) Haupts, U.; Maiti, S.; Schwille, P.; Webb, W. W. *Proc. Natl. Acad. Sci. U.S.A.* **1998**, *95*, 13 573−13 578.
(30) Weber, W.; Helms, V.; McCammon, J. A.; Langhoff, P. W. *Proc. Natl. Acad. Sci. U.S.A.* In press.
(31) Voityuk, A. A.; MichelBeyerle, M. E.; Rosch, N. *Chem. Phys. Lett.* **1998**, *296*, 269−276.